

Using passive microwave and optical remote sensing to monitor flood inundation in support of hydrologic modelling

Ticehurst, C.J.¹, P. Dyce¹ and J.P. Guerschman¹

¹ *CSIRO Land and Water, Black Mountain, Canberra*
Email: catherine.ticehurst@csiro.au

Abstract: This paper describes two applications of remote sensing flood inundation mapping in support of hydrologic models: mapping monthly flood extent in the lower Mekong Basin (Cambodia and Vietnam); and near-real time mapping of inundation in the lower Condamine-Balonne catchment (South Queensland). Passive microwave (Tropical Rainfall Measuring Mission's (TRMM) Microwave Imager (TMI) the Advanced Microwave Scanning Radiometer for EOS (AMSR-E)) and optical remote sensing data (MODerate resolution Imaging Spectroradiometer - MODIS) are used in these studies. Both optical and passive microwave datasets are sensitive to surface water enabling them to map flood events. The relatively high spatial resolution of the MODIS sensor (250m up to 1km pixel size), along with its frequent acquisition of twice daily, make it theoretically ideal for mapping flood inundation, however it is often subject to cloud cover particularly during flood events. This is why passive microwave has also been investigated. The disadvantage of passive microwave is its low spatial resolution (~5km up to 70km footprint), with the smaller footprint coming from the higher frequency bands which are also affected by atmospheric water vapour. However, when the MODIS and passive microwave data are combined, the disadvantages of both sensor technologies can be reduced.

For both applications, the higher spatial resolution of the MODIS data is utilized to interpret and develop a set of rules for mapping the mixed pixels in passive microwave data (i.e. where a pixel contains part water/part land in this case) using historical imagery for the same dates.

For the Mekong River study, since the flood events gradually occur over a six month period, 37 GHz TRMM imagery was composited into monthly images and flood extent mapped for 1999 to 2002. The MODIS 8-day composite MOD09A1 was used to map flood extent for 2000 to 2002. Linear relationships between modelled flood volume, using a water account model, and mapped flood extent were developed for the Tonle Sap Lake and the Lower Mekong Delta. When the TRMM and MODIS were correlated with modelled water volume, the dry year in 1999 from the TRMM data enabled a good relationship to be developed, while the MODIS imagery provided the most accurate flooded area.

For the Condamine-Balonne catchment, flood events are of shorter duration and more unpredictable, so near-real time monitoring is required. For this study, daily MODIS data were used to map water extent when available, and the passive microwave data (AMSR-E) were used when MODIS was unavailable due to cloud cover. The imagery was correlated to streamflow data and a simple model is being developed to map flood extent from gauged stream flow measurements in the absence of remote sensing data. These flood extent maps are then used in the Deltares' Flood Early Warning System (FEWS) as part of a hydrological flood forecasting system.

This paper focuses on the methods developed from the two case studies to map flood extent using a combination of passive microwave and MODIS imagery.

Keywords: *Flood mapping, passive microwave, MODIS*

1. INTRODUCTION

The ability of remote sensing technologies to identify surface water has been utilized for many tens of years. Mapping surface water from the air, or space, has allowed the potential to monitor the dynamics of hydrological events through space and time at a consistent level of accuracy. For mapping flood events, remote sensing imagery needs to be frequent enough to capture critical flood stages. Both optical/infrared and microwave remote sensing instruments have been used for mapping surface water through time. Optical imagery operates in the visible portion of the wavelength spectrum, but also includes the infrared and thermal regions. Microwave imagery operates in the longer wavelengths from less than a centimetre up to a metre (or frequencies from 89 GHz to 0.3 GHz respectively).

Different wavelengths have different responses to water in the landscape. Much of the literature shows that for optical imagery the infrared wavelength, particularly around 1.5-1.7 micrometres performs well for separating water from land (Overton *et al.*, 2006). Instruments such as Landsat have a relatively high spatial resolution (30m pixels) allowing for the detection of fine water bodies. However such imagery is not routinely collected on a global scale through time, making regular monitoring of flooding events difficult. Instruments such as the Advanced Very High Resolution Radiometer (AVHRR) and the more recent MODIS do collect data at daily/sub-daily intervals. Even with a poorer spatial resolution (1 km pixels), the AVHRR has been used to map water with reasonable success (Tanaka *et al.*, 2003). The MODIS sensors have a higher spatial resolution ranging from 250m up to 1km with a twice daily overpass through much of the world, which has also been used to map surface water (Sakamoto *et al.*, 2007).

A major disadvantage in using optical imagery for flood mapping is that flood events are often associated with cloud cover. This is the main reason that microwave sensors have been explored for their ability to map surface water. Synthetic Aperture Radar sensors have proven useful in mapping floods (Alsdorf *et al.*, 2007) but they are not routinely available at regional scales. However, passive microwave sensors acquire data at a high temporal frequency (1-2 times daily) on a near-global scale. Single bands have been used for mapping surface water (Tanaka *et al.*, 2000). However atmospheric water vapour content and temperature affect the brightness temperature at frequencies of 37GHz and higher, hence the vertical (V) and horizontal (H) polarization difference (ΔT) is often used for surface water mapping (Smith, 1997) and has been used for large floods (Sippel *et al.*, 1998). Kerr and Njoku (1993) recommend the Polarization Ratio [$PR = (TbV - TbH) / (TbV + TbH)$], where Tb is Temperature brightness] rather than the ΔT since it is less affected by the atmosphere and is independent of effective soil temperature. One of the large challenges in using passive microwave to map surface water is its large spatial footprint (5km up to 70km). Mixed pixel analysis is often used to determine the proportion of water within each flooded pixel based on theoretical or empirical estimates of the proportion of wet and dry surfaces (Mialon *et al.*, 2005).

Daily river stage or discharge has been correlated to inundation area as derived from regularly acquired remote sensing imagery. Even without ground data, these correlations can still show the shape and timing of seasonal hydrographs, and with ground measurements the absolute discharge can be estimated to within a factor of two (Smith, 1997). For microwave data, Choudhury (1989) achieved a linear correlation of $R = 0.8$ while Brakenridge *et al.* (2007) used a fourth order polynomial with an AMSR-E 36.5 GHz horizontal ratio achieving good results. Sippel *et al.* (1998) found mapped flooded area was correlated with river stage, using it to develop a predictive relationship for inundation patterns with historical stage records.

The following sections describe the two case studies to map flood extent using passive microwave and MODIS imagery: The Lower Mekong River and the Condamine-Balonne catchment. Passive microwave and MODIS data were selected since they acquire near-real-time imagery for most of the world's land mass at a daily frequency, are freely available, and contain archive data for historical analysis. The Lower Mekong River and the Condamine-Balonne catchment provide contrasting environments in terms of climate, flood extent and duration, therefore require different applications of the remote sensing data.

2. CASE STUDY 1: THE LOWER MEKONG RIVER

2.1. Methods

Flooding in the lower Mekong River (Figure 1) is seasonal in nature, occurring over a six-month period from around May to October. Flooding is most extensive around the Tonle Sap Lake in Cambodia and the Mekong Delta in Vietnam. Due to the slow nature of the flood event, and the high proportion of cloud cover, the remote sensing imagery was analysed at monthly intervals. For MODIS, the 8-day Surface Reflectance (MOD09A1) with a pixel size of 500m was used from 2000 to 2002. An Optical Water Index (OWI,

Guerschman *et al.*, 2008) was then used to map water extent in the MODIS images. The OWI is based on the relationship between the Enhanced Vegetation Index (EVI, equation 1) (Huete *et al.*, 2002) and Global Vegetation Moisture Index (GVMI, equation 2) (Ceccato *et al.*, 2002) such that the $OWI=0$ when $EVI \geq 0.2$ and $OWI=GVMI-EVI$ when $EVI < 0.2$. An OWI of ≥ 0.2 was adopted as water.

$$EVI = G \cdot \frac{\rho_{NIR} - \rho_{red}}{\rho_{NIR} + C_1 \cdot \rho_{red} - C_2 \cdot \rho_{blue} + L} \quad (1) \quad GVMI = \frac{(\rho_{NIR} + 0.1) - (\rho_{SWIR2} + 0.02)}{(\rho_{NIR} + 0.1) + (\rho_{SWIR2} + 0.02)} \quad (2)$$

The TRMM satellite has been in operation since late 1997, allowing an overlap with the MODIS data. The Level 1B11 Tb swath data for 1998 to 2002 were geometrically projected into latitude/longitude with a pixel size of 10 km x 10 km. The Tb at 37 GHz (horizontally polarised band) is used to map surface water since it provides the best balance between spatial resolution and atmospheric interference effects (Brakenridge *et al.*, 2007). A rainfall mask of 85 GHz vertical minus 22 GHz vertical (Ferraro *et al.*, 1998) was also applied to the imagery to help remove these effects from the data. The remaining data were then composited into a monthly image using the lowest Tb value to capture the most water. A cloud-free scene was then selected from the MODIS 16-day MOD43B dataset to determine a set of rules for mixed water/non-water pixels in the TRMM data. The 16-day product has been corrected for variations due to sun angle, making it a cleaner image than the 8-day (MOD09A1) product. (It could not be routinely used for flood mapping of the Mekong River due to frequent cloud cover which restricted application of the sun angle correction resulting in lots of null data in many of the scenes). A TRMM composite image was used for the same 16-day period. The OWI was calculated for the MODIS scene providing a water mask, before being resampled to match the TRMM pixels. This aggregate resampling process gave the proportion of water (based on MODIS) within each corresponding TRMM pixel. The MODIS water proportion was plotted against the TRMM Tb before a third order polynomial was fitted against the curve and used to threshold the TRMM Tb into proportion of water.



Figure 1. Lower Mekong River.

2.2. Results

The images in Figure 2 show the areas across the Mekong Delta identified as water. Tonle Sap can be seen in the north western corner, the coast of the Gulf of Thailand is in the south west and the Mekong Delta flows in to the South China Sea in the south west. The 10th June image shows the initial dry season extent of the Tonle Sap. The series shows increasing inundation as the flood fills the lake and the Mekong Delta. Initial validation has shown that the OWI threshold of 0.2 tends to exclude significant areas of ‘mixed pixels’ which are also influenced by vegetation, soil on shorelines, or water discolouration. Further work on validation is required to improve and refine this classification. However, for the Lower Mekong the measured flooded area in the dry seasons return to virtually the same level for the three years observed in both areas. This helps support the consistency of the OWI classification with MODIS over time.

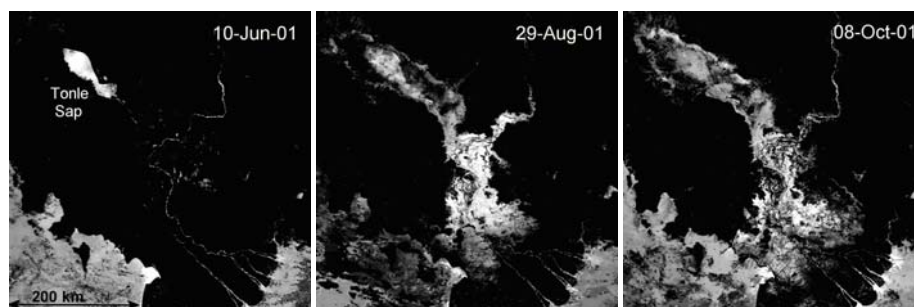


Figure 2. MODIS flood extent during the 2001 Wet Season. Fully flooded pixels appear as grey to white.

Both the MODIS and TRMM have advantages in their ability to map surface water for the Lower Mekong River. The MODIS pixel size of 500 m x 500 m shows fine detail that is not evident in the TRMM 10 km x 10 km pixels. However, the TRMM sensor is less affected by cloud cover due to its longer wavelengths. Hence, the MODIS and TRMM data points were compared, to determine the best relationships to use with modelled water volumes derived from a water accounting model (Eastham *et al.*, 2008). Figure 3 shows the TRMM (2000-2002) and MODIS (2000-2002) monthly flood extent for Tonle Sap, plotted against the

modelled Tonle Sap water volumes. There is a linear relationship between the TRMM extent and modelled storage ($R^2 = 0.89$, $RMSE = 873 \text{ km}^2$) as well as the MODIS extent and modelled storage ($R^2 = 0.76$, $RMSE = 2047 \text{ km}^2$). However, there is a large difference in flood extent with the TRMM having a maximum area around $10,000 \text{ km}^2$ while the MODIS is around $15,000 \text{ km}^2$.

Independent research (MRC, 2007) has mapped the Tonle Sap flood extent covering a similar area to those produced by the MODIS data. Given this information, it appears that the TRMM is most likely underestimating flood extent due to mixed water/non-water pixels, while the MODIS is giving a more realistic estimate. This is expected since the MODIS data has a higher spatial resolution, and hence can map more detail. However, the TRMM has a better R^2 and RMSE than the MODIS flood extent. This may be due to increased cloud cover occurring during wetter periods, and hence limiting the number of MODIS scenes available for mapping flood extent. For Tonle Sap, the monthly data for the TRMM and MODIS for 2000 to 2002 were regressed against each other (a linear relationship with R^2 of 0.89 and $RMSE = 96 \text{ km}^2$). This relationship was used to scale the TRMM data (1998-2002) up to MODIS (2000 to 2002) so both datasets could be used to generate a relationship between modelled monthly flow data and flood extent as measured by remote sensing imagery.

Both the optical and passive microwave remote sensing data show a relationship with modelled water volume when they are used to mapped flood water extent. The TRMM flood extent measurements were better correlated to the modelled water volume through time compared to MODIS. However the MODIS flood extent was more accurate in its absolute value. The results indicate that the passive microwave may be a suitable method for mapping monthly flood extent in Tonle Sap as it is less influenced by cloud cover compared to optical instruments. However an adjustment is required, using a higher resolution sensor like MODIS, to scale the measured flood extent.

3. CASE STUDY 2: THE CONDAMINE-BALONNE RIVER

3.1. Methods

The Condamine-Balonne catchment is situated in Southeast Queensland, Australia (Figure 4). The area of interest is south of the township of St George to the Queensland border, where flooding mostly occurs due to upstream rainfall events. Water in this area is heavily regulated, with water extracted from the river and stored in ring tanks for irrigation purposes when there are sufficient flows. Flood events occur on a much shorter time-frame than the Mekong River, days rather than months, with the floodplain covering only 3800 km^2 . It is for these reasons that daily remote sensing imagery was required for mapping flood events, with an emphasis on mixed pixel analysis especially for the large spatial footprint of passive microwave imagery.

This study uses daily daytime 500m reflectance MODIS imagery (MOD09A1), giving up to two overpasses a day depending on its swath track. For the MODIS imagery, the Optical Water Likelihood was used (Guerschman *et al.*, 2008). The OWL uses the OWI and is based on a sigmoid function resulting in a number between zero and one based on the likelihood of there being water present. Since the images are still subject to cloud cover, the accompanying MODIS quality band information was used to mask the cloud pixels. Apart from null data, the remainder of the image consisted of values ranging from 0 to 100, representing the percentage of water within a pixel. The two MODIS scenes for each day were combined, such that clouds and null pixels were replaced by the other scenes if it had real data. Where there was real data from both overpasses, the average value was used to help reduce any variation in illumination due to the different sun angle as well as help reduce any noise in the imagery.

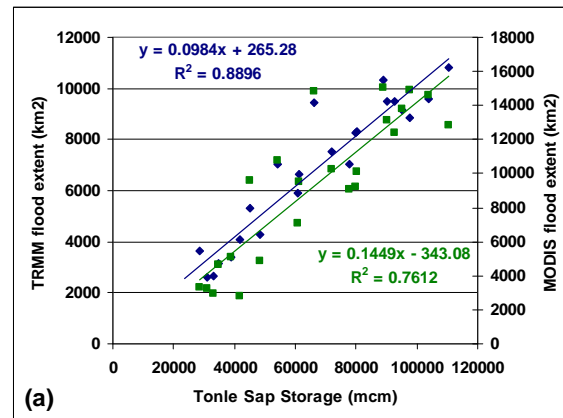


Figure 3. Scatterplot of TRMM (1998-2002) (blue) and MODIS (2000-2002) (green) mapped flood extent versus modelled monthly storage water volume in mcm (mega-cubic metres) for Tonle Sap. The left and right y-axis shows the TRMM and MODIS flood extent respectively.

The AMSR-E passive microwave instrument data (Ashcroft *et al.*, 2006) were used here since it has a slightly better spatial resolution than the TRMM and a wider swath for better coverage. Since the data comes from varying times of the day, the PR was used on the 37 GHz band (Kerr and Njoku, 1993). The same rain mask as the Mekong Study was applied. The 37 GHz PR image was still influenced by the proportion of vegetation cover, creating particular confusion between surface water and bare soil. To help reduce this effect, a desert correction was applied based on the threshold by Grody (1991) which uses the 18 GHz vertical minus horizontal value, but here we used the near-linear relationship between the 37 GHz PR and the 18 GHz V-H to correct for the variation in the 37 GHz PR band (where the corrected 37 GHz PR = 37 GHz PR - 0.00144 x (18GHz V-H)). The relationship was near-linear because the 37 GHz PR was more sensitive to water pixels than the 18 GHz data, particularly for the finer water features which were more difficult to detect in the 18 GHz data due to its larger spatial footprint of 28 x 16 km.

Like the Mekong case study, a MODIS water image (produced from the OWI) was used to develop a relationship between the corrected PR and proportion of water within each pixel. For this case study, a single MODIS image acquired at the same time as the AMSR-E image was used. It included a large flood in southwest Queensland, which meant there were AMSR-E pixels having up to 100% water in them. Unlike the Mekong case study where mixed pixel thresholds were used, a linear relationship (Water proportion = corrected 37 GHz PR x 24.3 + 0.010, $R^2 = 0.42$, RMSE = 0.0056 PR) was adopted instead as it provided a continuous relationship with water proportion. (The low R^2 was mostly due to sub-pixel misregistration of the MODIS and AMSR-E images). The final AMSR-E water product was a combination of all images for the day that covered any part of the catchment, which were combined in a similar way to the MODIS water products.

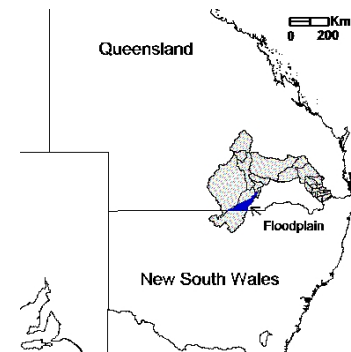


Figure 4. Location of Condamine-Balonne catchment (shaded region)

Since the AMSR-E pixel was much larger than the MODIS, and these data are to be combined (described below), a 90m Shuttle Radar Topographic Mission DEM (Slater *et al.*, 2006) which had striping removed and voids filled by John Gallant's group at the CSIRO, was used to distribute water within each AMSR-E pixel. To do this, a mathematical flat surface was fit to all the DEM pixels within an AMSR-E pixel. This mathematical surface was then subtracted from those DEM pixels to remove the large topographic features while retaining the finer features, such as the relatively low points. The proportion of water within each AMSR-E pixel was then distributed into the lowest pixels of the flattened DEM. This process was applied to each AMSR-E pixel. The reason why this flat surface correction was applied was to flood the relatively low sections within each AMSR-E pixel rather than have the water pooling in the absolute lowest points, since water moves dynamically through the landscape filling the relatively lowest sections as it reaches them. The DEM-filled AMSR-E water product was then resampled to the MODIS pixel size.

The MODIS and AMSR-E water products were then combined such that the MODIS data were used unless there were clouds or null pixels (Figure 5). The AMSR-E water product replaced the MODIS cloud and null pixels when it contained real data. It must be noted that microwave data are not totally immune to cloud cover, they are affected by precipitating clouds, particularly the higher frequency data. However, with three independent overpasses (MODIS Terra ~ 10.30am, MODIS AQUA and AMSR-E ~ 2pm, AMSR-E ~ 2am) there is more chance for rain free imagery in the areas of interest.

3.2. Results

These products are used in the Deltares' Flood Early Warning System (Delft-FEWS) software as an independent source of flood extent for comparison with the hydrological models generated within this flood forecasting system. Work is now beginning on the validation of the water extent products. Initial visual comparison between flood extents as mapped in the lower-Balonne floodplain compared well with the work of Apan and Stern (2006). However a thorough quantitative validation analysis is required. Current work also includes linking it to daily flow gauge data. The goal of this is to establish a strong relationship between in-situ flow gauge data and mapped flood extent, such that the flow gauge data can be used to predict flood extent in the absence of remote sensing imagery. Initial results show there is some relationship between flood volume (from the State of Queensland (Department of Natural Resources, Mines and Water) 2009) and mapped flood extent for the lower Balonne floodplain (Figure 6). There appears to be a lag between the peak in flood volume *i.e.* the total volume of water passing a point, and the mapped water extent. In particular

there is a rapid increase in mapped flood extent occurring after the water volume increase. Following the initial increase, the flood extent varies little compared to flood volume. Some of this may be related to the remnant wet soil, natural barriers such as river banks which contain the water until it overflows, or irrigation ring tanks filling during times of rain or flood, and adjustments will need to be made for this.

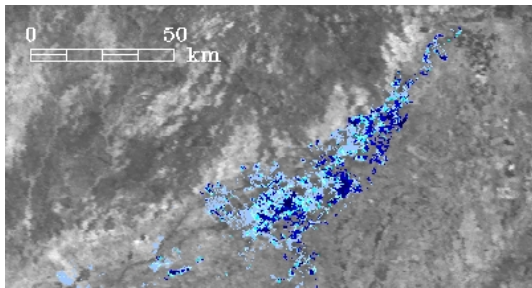


Figure 5. Example of flood map for the lower Balonne floodplains. Light blue represents small proportion of water within a pixel, darker colours represent a large proportion.

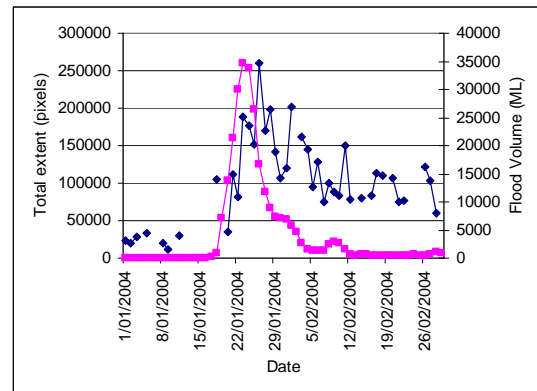


Figure 6. Measured flood volume* (pink) and flood extent mapped using remote sensing (blue) for January/February 2004.

4. DISCUSSION AND CONCLUSIONS

This study has developed two different ways of using optical and passive microwave remote sensing imagery for mapping floods to help reduce the effects of cloud contamination, and optimize the data's spatial resolution and temporal frequency to suit the size and duration of the flood events. Incorporation of these temporal remote sensing datasets with flood volume or stream flow data as part of a hydrological model was also demonstrated. One disadvantage of the large pixel size of the microwave data occurs when mapping small flood events such as those in the Condamine-Balonne, however when there are no other data available it may be used to help fill in the gaps, particularly during critical times when cloud cover is limiting the use of optical imagery. For large floods such as those in Tonle Sap, the TRMM data did perform well with respect to the modelled water volume through time, however its absolute flood extent was too low and hence requires the higher resolution of the MODIS to correct for this. There is always a compromise when using near-real time daily imagery compared to the higher level composite products. This is especially true when using the MODIS daily product, compared to a more refined 16-day composite product which has nearly all clouds removed and is corrected for illumination variations from the sun. The near-real time water product will contain greater variability and noise, but these effects can be reduced somewhat by combining all images from one day.

Both of our studies have linked the mapped flood extent to flow data. Linking flood inundation extent to gauge height only works well for rivers of relatively constant discharge over extended periods, rather than sharp peaks, unless the imagery were at daily intervals (Frazier *et al.* 2003). Hence the two different methods used to map flood extent on different time-scales were suited to the nature of their respective flood events and for linking with flow data. Once a relationship has been established between mapped flood extent and in-situ gauge data, they can provide support to hydrological models through independent comparison and assessment as well as a method for mapping and visualizing the water extent once linked to modelled flow data.

The Mekong River case study was based on a very large, seasonal flood event that lasted for six months and covering some 15000 km² for Tonle Sap, while the Condamine-Balonne experienced much shorter duration flood events covering less than 4000 km². In both studies, the MODIS data were used due to its better spatial resolution, while the passive microwave imagery was used due to its lower sensitivity to cloud cover. While an initial visual comparison with independent flood maps does give some confidence in their quality, the next major stage of our research is the quantitative validation of these flood extent maps with the intention of a follow-up paper detailing these results and reporting on the operational potential of these methods.

ACKNOWLEDGEMENTS

This work is part of the water information research and development alliance between CSIRO's Water for a Healthy Country Flagship and the Bureau of Meteorology. This work was also part of the Mekong River

* Based on or contains data provided by the State of Queensland (Department of Natural Resources, Mines and Water) [2009]. In consideration of the State permitting use of this data you acknowledge and agree that the State gives no warranty in relation to the data (including accuracy, reliability, completeness, currency or suitability) and accepts no liability (including without limitation, liability in negligence) for any loss, damage or costs (including consequential damage) relating to any use of the data. Data must not be used for direct marketing or be used in breach of the privacy laws.

Basin Resources Assessment project in the Water for a Healthy Country Flagship. The authors wish to thank the reviewers for their valuable comments.

REFERENCES

- Alsdorf, D. E., P. Bates, J. Melack, M. Wilson, and T. Dunne (2007), Spatial and temporal complexity of the Amazon flood measured from space, *Geophys. Res. Lett.*, 34, L08402, doi:10.1029/2007GL029447.
- Apan, A., and Sternes, P. (2006), Mapping and spatio-temporal analysis of flooded and inundated areas in the Lower Balonne Floodplain, Queensland, Australia. *WSEAS Transactions on Environment and Development*, 4(2), 360-367.
- Ashcroft, P., Wentz, F. (2006), updated daily. *AMSR-E/Aqua L2A Global Swath Spatially-Resampled Brightness Temperatures V002*, [Jan-Feb 2004]. Boulder, Colorado USA: National Snow and Ice Data Center. Digital media.
- Brakenridge, G.R., Nghiem, S.V., Anderson, E., Mic, R. (2007), Orbital microwave measurement of river discharge and ice status. *Water Resources Research*, 43, W04405, 16pp.
- Ceccato, P., Gobron, N., Flasse, S., Pinty, B., Tarantola, S. (2002), Designing a spectral index to estimate vegetation water content from remote sensing data: Part I Theoretical Approach. *Remote Sensing of Environment*, 82, 188-197.
- Choudhury, B.J. (1989), Monitoring global land surface using Nimbus-7 37 GHz data: Theory and examples. *International Journal of Remote Sensing*, 10(10), 1579-1605.
- Eastham, J., Mpelasoka, F., Mainuddin, M., Ticehurst, C., Dyce, P., Hodgson, G., Ali, R., Kirby, M. (2008), Mekong River basin water resources assessment: Impacts of climate change. *CSIRO: Water for a Healthy Country National Research Flagship*.
- Ferraro, R.R., Smith, E.A., Berg, W., Huffman, G.J. (1998), A screening methodology for passive microwave precipitation retrieval algorithms. *Journal of the Atmospheric Sciences*, 55, 1583-1600.
- Frazier, P., Page, K., Louis, J., Briggs, S., Robertson, A.I. (2003), Relating wetland inundation to river flow using Landsat TM data. *International Journal of Remote Sensing*, 24(19), 3755-3770.
- Grody, N.C. (1991), Classification of snow cover and precipitation using the Special Sensor Microwave/Imager (SMM/I). *Journal of Geophysical Research*, 96, 7423-7435.
- Guerschman, J.P., Van Dijk, A.I.J.M., McVicar, T.R., Van Niel, T.G., Lingtao, L., Lui, Y., Peña-Arancibia, J. (2008), Actual evapotranspiration and water balance estimates from satellite observations over the Murray-Darling Basin. Canberra, *CSIRO Science Report*.
- Huete, A., Didan, K., Muiira, T., Rodriguez, E.P., Gao, X., Ferreira, L.G. (2002), Overview of the radiometric and biophysical performance of the MODIS vegetation indices. *Remote Sensing of Environment*, 83, 195-213.
- Kerr, Y.H., and Njoku, E.G. (1993), On the use of passive microwaves at 37 GHz in remote sensing of vegetation. *International Journal of Remote Sensing*, 14(10), 1931-1943.
- Overton, I.C., McEwan, K., Gabrovsek, C., Sherrah, J.R. (2006). The River Murray Floodplain Inundation Model – Hume Dam to Lower Lakes. *CSIRO Water for a Healthy Country Technical Report 2006*. CSIRO: Canberra.
- Mialon, A., Royer, A., Fily, M. (2005), Wetland seasonal dynamics and interannual variability over northern high latitudes, derived from microwave satellite data. *Journal of Geophysical Research*, 110, D1712, doi:10.1029/2004JD005697.
- MRC (2007), Annual Mekong Flood Report 2006. *Mekong River Commission*, Vientiane, 76pp.
- Sakamoto, T., Nguyen, N.V., Kotera, A., Ohno, H., Ishitsuka, N., Yokozawa, M. (2007), Detecting temporal changes in the extent of annual flooding within the Cambodia and the Vietnamese Mekong Delta from MODIS time-series imagery. *Remote Sensing of Environment*, 109, 295-313.
- Slater, J.A., Garvey, G., Johnston, C., Haase, J., Heady, B., Kroenung, G., and Little, J. (2006), The SRTM data "finishing" process and products. *Photogrammetric Engineering and Remote Sensing* 72 (3), 237-247.
- Smith, L.C. (1997), Satellite remote sensing of river inundation area, stage, and discharge: A review. *Hydrological Processes*, 11, 1427-1439.
- Sippel, S.J., Hamilton, S.K., Melack, J.M., Novo, E.M.M. (1998), Passive microwave observations of inundation area and the area/stage relation in the Amazon River floodplain. *International Journal of Remote Sensing*, 19(16), 3055-3074.
- Tanaka, M., Sugimura, T., Tanaka, S., Tamai, N. (2003), Flood-drought cycle of Tonle Sap and Mekong Delta area observed by DMSP-SSM/I, *International Journal of Remote Sensing*, 24(7), 1487-1504.
- Tanaka, M., Sugimura, T., Tanaka, S. (2000), Monitoring water surface ratio in the Chinese floods of summer 1998 by DMSP-SSM/I. *International Journal of Remote Sensing*, 21(8), 1561-1569.